Earthquakes and Structures, *Vol. 8, No. 5 (2015) 1039-1054*
DOI: http://dx.doi.org/10.12989/eas.2015.8.5.1039

Cyclic testing of weak-axis column-tree connections with formation of plastic hinge at beam splice

Keunyeong Oh, Liuyi Chen, Sungbin Hong, Yang Yang and Kangmin Lee*

Department of Architectural Engineering, Chungnam National University, Daejeon, Korea

(Received May 8, 2014, Revised December 16, 2014, Accepted December 27, 2014)

Abstract. The purpose of this study was to evaluate the seismic performance of weak-axis column-tree type connections used in steel moment frames. These connections are composed of a shop-welded and field-bolted steel structure and can improve welding quality. On this basis, column-tree type connections are widely used in steel moment resisting frames in Korea and Japan. In this study, splices designed with a semi-rigid concept regarding the seismic performance of column-tree connections were experimentally evaluated. The structures can absorb energy in an inelastic state rather than the elastic state of the structures by the capacity design method. For this reason, the plastic hinge might be located at the splice connection at the weak-axis column-tree connection by reducing the splice plate thickness. The main variable was the distance from the edge of the column flange to the beam splice. CTY series specimens having column-tree connections with splice length of 600 mm and 900 mm were designed, respectively. For comparison with two specimens with the main variable, a base specimen with a weak-axis column-tree connection was fabricated and tested. The test results of three full-scale test specimens showed that the CTY series specimens successfully developed ductile behavior without brittle fracture until 5% story drift ratio. Although the base specimen reached a 5% story drift ratio, brittle fracture was detected at the backing bar near the beam-to-column connection. Comparing the energy dissipation capacity for each specimen, the CTY series specimens dissipated more energy than the base specimen.

Keywords: column-tree type; weak-axis connections; cyclic testing; bolt slip; beam splice

1. Introduction

Moment resisting frames have been widely used in many steel building structures, and have been recognized as one of the best structural systems to resist lateral loads. Basic components such as beams, columns, and panel zones exhibit large deformation capacity and dissipate energy without significant loss of strength and failure in connections. In order to improve construction quality and allow the use of a modular technique, column-tree type connections are more frequently used in beam-to-column moment connections in Korea and Japan.

In a column-tree connection system as shown in Fig. 1, a stub beam made with a short girder is usually welded to the column in the shop first. This approach provides economical and quality welding and easy inspection (Mahin 1998, Miller 1998). After the column is installed in the field,

*Corresponding author, Associate Professor, E-mail: leekm@cnu.ac.kr

 ISSN: 2092-7614 (Print), 2092-7622 (Online)

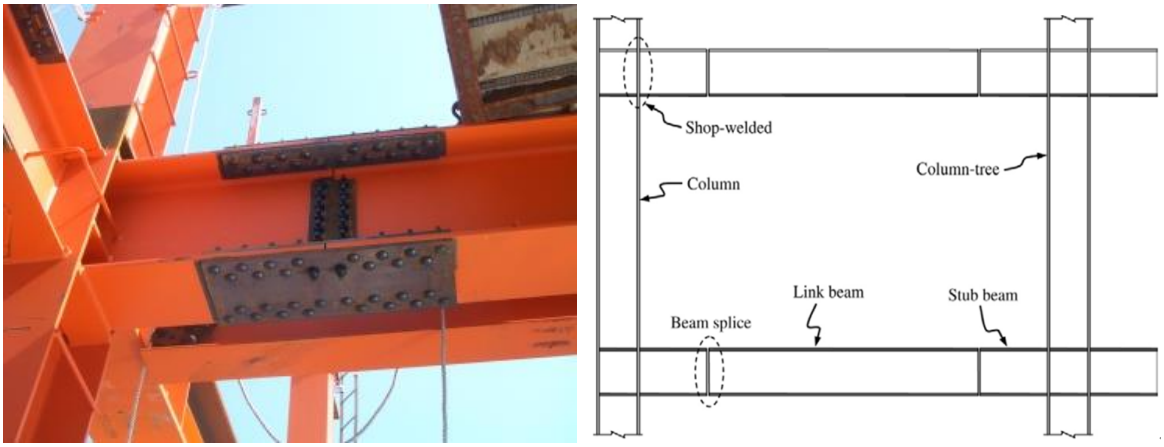

(a) The detail of splice connections (b) Overview of column-tree type system

Fig. 1 Typical column-tree connection system

the middle link beam and splices are fully bolted to the end of the stub beam. The use of the field bolted splice connection can speed up construction and reduce construction expenses.

Traditionally, splice connections are designed such that they are not weaker than the stub beam in order to ensure adequate stiffness according to the full-strength design principle. Furthermore, the splice connections are considered as part of the whole and do not play an important role in seismic performance in a frame under earthquake loads. The formation of a plastic hinge hence mostly occurs in the stub beam. Like pre-Northridge field-welded moment frames, unexpected brittle and early fracture of column-tree connections were also observed before the story drift ratio reached 0.03 rad in the experiment (Lee *et al.* 1998). The failure mode of these specimens was fracture at the stub beam flange. Fully bolted splice connections did not improve the performance because the weld metal and the root opening of the flange did not exhibit ductility under restrained conditions.

A semi-rigid column-tree moment resisting frame system was proposed (McMullin 2003) in a recent study. In the proposed semi-rigid column-tree system, the splices were designed to be semi-rigid to utilize the ductility capacity and energy dissipation. The results showed that the semi-rigid column-tree system is reliable and maintains large seismic resisting capacity. In addition, stiffness can be adjusted to reduce seismic forces and improve the deformation capacity.

Another advantage of semi-rigid frames is that the natural periods of a structure can be controlled and they can limit the magnitude of bending moment applied to the beam-to-column joint. In other words, a semi-rigid steel frame is designed to dissipate energy and return to a static state. To simulate the axial load that results in the plates from beam bending, the strength and ductility of the flange plate specimen under purely axial tension and compression were measured in the experiment. The test results indicated that the splice plates exhibited stable hysteretic behavior and bolt slip was a reliable source of energy dissipation.

Two column-tree connections with weakened beam splices were tested by (Lee *et al.* 2014) and the test results showed that reducing the portion of the splice plate area had almost no effect on the stiffness and strength before failure. However, the capacity of energy dissipation was better than that of traditional column-tree connections. Note that it was also observed that the bolt slip prevented the development of flange plate yielding.

2. Design program

2.1 Design concept of specimens

The main objective of this test project was to investigate the cyclic performance of weak-axis column-tree connections with assumption that a plastic hinge is formed at the stub beam.

Moment resisting frame systems must resist lateral forces and develop large ductile deformation. These frames are designed such that seismic energy imported to the frames can be dissipated by yielding of the material near the plastic hinge (the panel zone can then be ignored because of weak-axis connections). In other words, the safety of such structures mainly depends on the capability to absorb energy in the inelastic range rather than the elastic stiffness of the structures. Therefore, by reducing the splice plate cross-sectional area, weak-axis column-tree connections where a plastic hinge is formed in the splice connection are proposed in this paper. The rationale for this can be explained as follows:

1. Compared with the deformation capacity in the aforementioned tests, column-tree connections designed with semi-rigid exhibited better performance than that of traditional connections. However, the response of a semi-rigid frame is more complex, as the location of plastic hinge formation may shift back and move between the stub beam and the splice connection. According to the recommended or practiced location of the plastic hinge, it is difficult to determine the cross-sectional area and number of bolts at the splice.

2. In general, it is recommended that the beam splice connection be placed near the inflection point on the moment curvature or at 1/8 to 1/6 of the span length. The location of the splice connection in the proposed design concept may allow a more flexible layout. Splice connections can be utilized to provide more plastic rotation and stable energy dissipation capacity because pre-tensioned bolts are ductile components (Astaneh-Asl 1996, 1997).

2.2 Design of specimens

The specimens were fabricated using hot-rolled H section steel. Base specimen was fabricated with H-600×200×11×17 SS400 steel at the beam and H-400×400×13×21 SM490 steel at the column. Other specimens were fabricated with H-600×200×11×17 SHN400 steel at the beam and H-400×400×13×21 SHN490 steel at the column. SN steel is known to offer better seismic performance than rolled steel for general structures. Pre-tensioned high-strength bolts of M20-F10T were used at the splice connection. The member sizes were chosen such that the beam flanges width would be narrower than the column depth.

The design of base specimen was based on the widely used pre-Northridge weak-axis connections. The continuity plates were welded to column flanges and the web. The shear plate was welded to the continuity plates and the column web. The beam flanges and web were shop welded to the corresponding continuity plates and shear plate. The steel backing bars were left in place on both the top and bottom beam flanges, as shown in Fig. 2. The beam splice was located at a distance of 1,100 mm from the column web. Adopting the full-strength design method, the flange splice plates are adequate to carry the maximum design moment and the web plates are designed to carry the total shear and portion of moment caused by the eccentric shear force. The eccentric distance was calculated from the centerline of the beam splice to the centroid of one side bolt group.

Kim *et al.* (2004) tested 14 specimens to compare their behavior with that of existing weak-axis

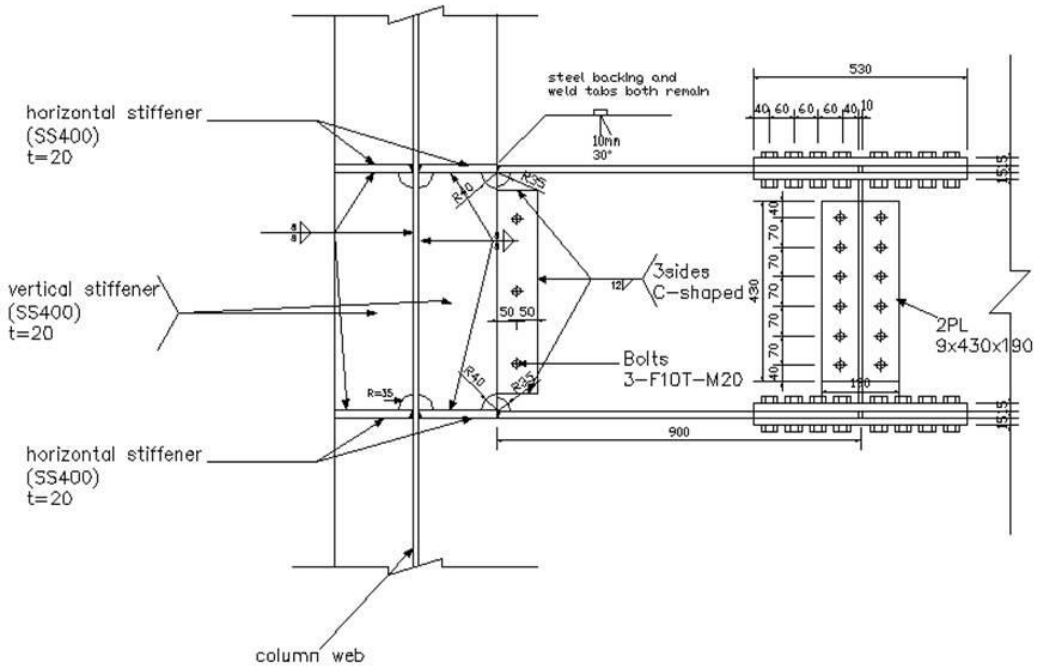

Fig. 2 Details of base specimen

connections and the effect of bolt quantity. Test results showed that the BA (column-tree type) specimen exhibited large deformation, stable energy dissipation capacity, and simple constructability. Based on this, the beam-to-column joint of CTY specimens was different from that of base specimen. The stub beam flanges and web were directly welded to the column web and two stiffener plates located close to the stub beam were welded to the column flanges, which were also welded to the stub beam flange. These two stiffener plates were assumed to carry the entire bending moment and shear. Considering constructability, the backing bars were left.

CTY specimens were designed such that the beam splice connection was attained by reducing the cross-sectional area of the splice plates. Accurate calculation of the beam splice was adapted from the reduced beam section (RBS) concept and could shift the plastic hinge to the splice connection. A plastic hinge is expected to form at the centerline of the splice plate within the length of the flange splice plate. The moment at the face of the column is computed as follows

$$M_f = M_{pr} + V_{pr}S \tag{1}$$

$$V_{pr} = \frac{2M_f}{l-2S} \tag{2}$$

$$M_{pe} = R_y F_y Z_x \tag{3}$$

where, M_f is the probable maximum moment at the column face under the service load, S is the distance from the column face to the center of the splice plate, V_{pr} is the designed shear of the splice under the service load, M_{pr} is the designed moment of the splice under the service load, and M_{pe} is the expected moment strength of the unreduced beam section at the column.

The CTY group contains two specimens, CTY600 and CTY900. The main variable is the

location of the beam splice. The numbers denote the distance from the edge of the column flange to the center of the beam splice plate. In order to determine the designed moment and shear at the beam splice, the ratio of M_f/M_{pe} was designed to be 0.95, which means the reduced level compared with the expected moment at the column face. The equations show that the distance from the column to the center of the beam splice gradually becomes smaller, the designed moment would increase at the beam splice and the cross-sectional area of the splice plates would increase correspondingly. To ensure stability of the splice connection, the cross-sectional area of the web splice plates was adequate of each specimen, and was assumed to carry the total shear.

Hisashi Okada *et al.* (2001) studied the distribution of the bending moment between flange splice plates and web splice plates. The results showed that the distribution was related to the inertia moment of the beam web and the inertia moment of the beam section expressed as follows

$$M_{ws} = \varphi M_{pr} \frac{I_w}{I_b} \tag{4}$$

$$M_{pr} = M_{fs} + M_{ws} \tag{5}$$

where, φ is the moment transfer ratio to the web splice and is equal to 0.4 in general. M_{ws} is the portion of the designed moment of the splice carried by web splice plates, M_{fs} is the portion of the designed moment of the splice carried by flange splice plates, M_{pr} is the designed moment of the splice under service load, I_w is the inertia moment of the beam web, and I_b is the inertia moment of the beam cross section. This equation is suitable for determining the distribution of the moment before yielding of the splice plates. Under ultimate conditions, it is also necessary to check rupture over the effective net area and bearing at the bolt holes.

Each specimen satisfied the panel zone strength requirement. For weak-axis moment connections the design panel zone shear strength was calculated using the nominal yield strength, and the panel zone shear demand used the expected shear strength at the tips of column flange. All specimens satisfy the strong column-weak beam requirement given by AISC seismic provisions in the following equation

$$\frac{\sum M_{pc}^*}{\sum M_{pb}^*} \geq 1.0 \tag{6}$$

where, $\sum M_{pc}^*$ is the sum of the moments in the column above and below the joint at the intersection of the beam and column centerlines. $\sum M_{pb}^*$ is the sum of the moment in the beams at the intersection of the beams and column centerlines.

Details of CTY600 and CTY900 specimens are shown in Fig. 3. All specimen configurations are summarized in Table 1.

Table 1 Column-tree connection specimens

Specimen	Location of beam splice (mm)	Flange splices			Web splice	
		Flange plates		Bolts	Web plates	Bolts
Base	900	Top	PL-15×200×530	32	PL-9×190×430	12
		Bottom	2PL-15×70×530			
CTY600	600	Top	PL-11×200×530	32	PL-9×190×430	12
		Bottom	2PL-11×70×530			
CTY900	900	Top	PL-10×200×530	32	PL-9×190×430	12
		Bottom	2PL-9×70×530			

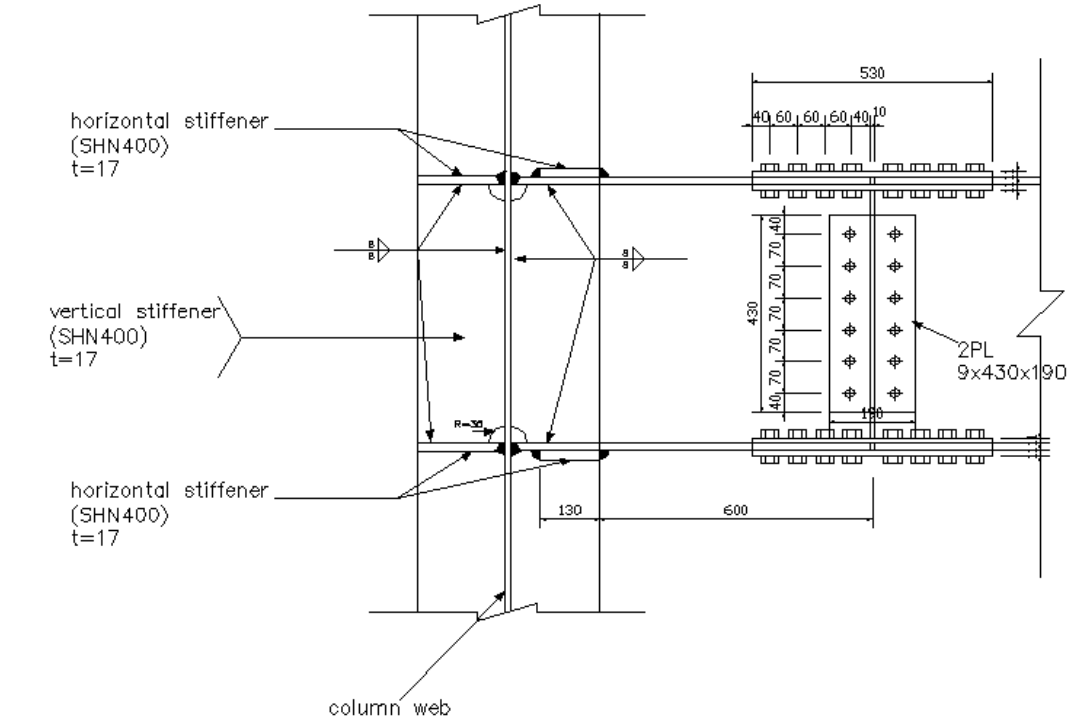

(a) CTY600

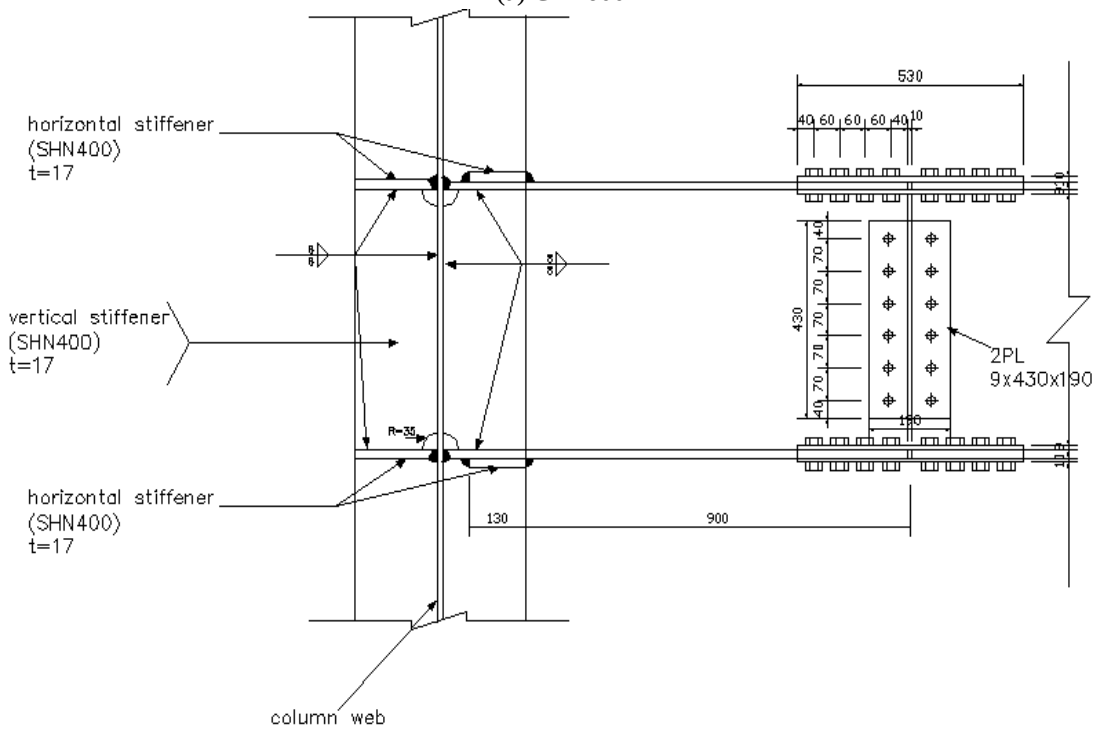

(b) CTY900

Fig. 3 Details of CTY series specimens

3. Experimental program

3.1 Material properties

Tensile test specimens were manufactured in accordance with KS B 0801(2007). The webs and flanges of different steel types were tested respectively. The test results are presented in Table 2. The actual yield strength (F_{ye}) of each coupon exceeded the nominal yield strength (F_y).

3.2 Test sets up, loading sequence and intrumentation

Fig. 4 shows an overall view of the test setup. All specimens consisted of a cantilever beam connected to a column web. The column was rotated 90 degrees and horizontally strongly fixed on the laboratory floor. The free end of the beam was pin-connected to the actuator. Lateral support was set up and provided out-of-plane stability to prevent beam twisting.
All the test specimens should be subjected to cyclic loading according to the requirements prescribed in the AISC seismic provisions. The applied quasi-static cyclic tests must be conducted by controlling the inter-story drift angle. The loading sequence is specified in Fig. 5. The loading was stopped when the entire loading sequence was completed, fracture occurred, or there was more than a 20% loss of strength.

Table 2 Coupon test results

Shape	Location	Steel	F_y (MPa)	F_u (MPa)	F_{ye} (MPa)	F_{ue} (MPa)
H-400×400×13×21(column)	Web	SHN490	325	490	398.4	559.7
	Flange	SHN490	325	490	407.9	571.4
H-600×200×11×17(beam)	Web	SHN400	235	400	336.3	470.5
	Flange	SHN400	235	400	292.3	455.8

Note: The 0.2% offset method was used for determining the yield strength of steel.
F_y and F_u are the nominal values, and F_{ye} and F_{ue} are the measured values

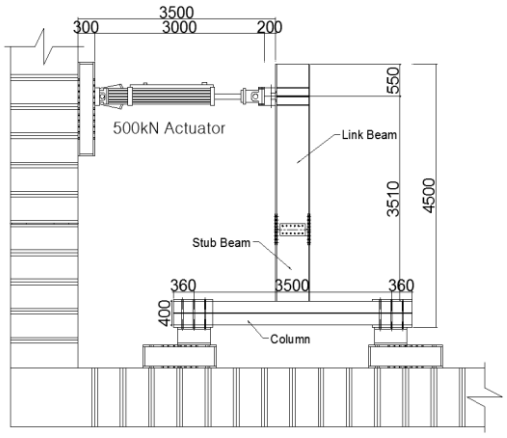

Fig. 4 Test setup

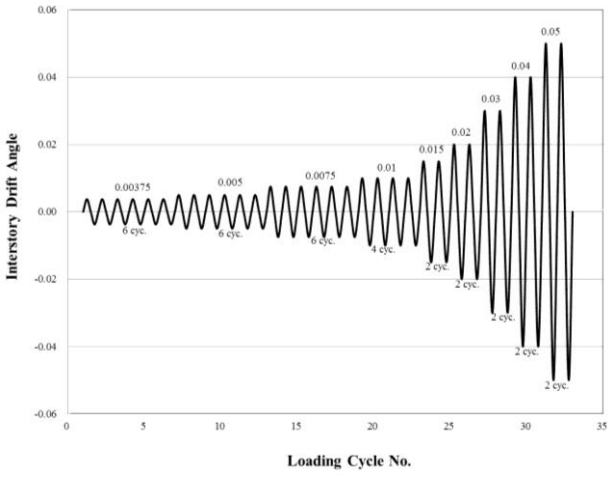

Fig. 5 Loading sequence

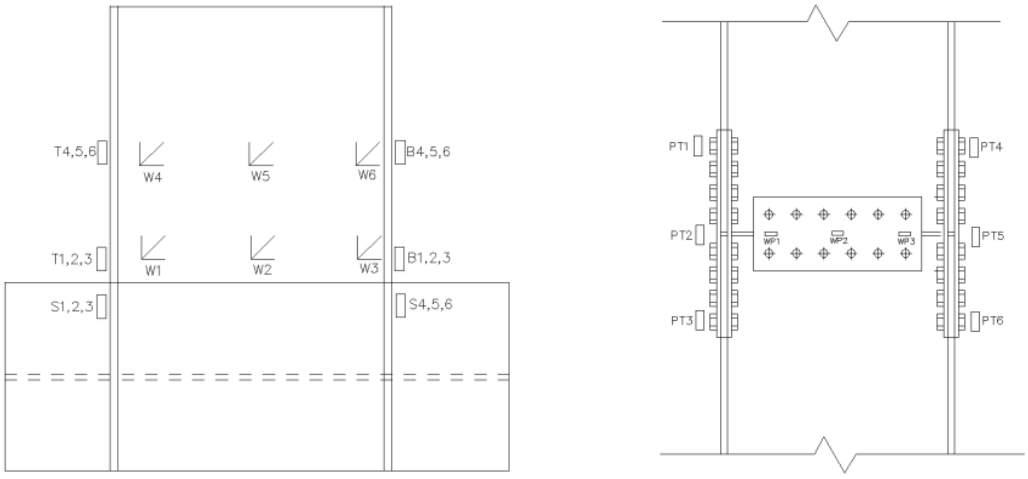

Fig. 6 Layout of strain gauges

Linear varying displacement transducers (LVDTs) were installed at both column stiffeners and the middle of the beam splice to measure the specific displacement of each specimen. Strain gauges were placed in specific locations on the specimens to measure local responses as shown in Fig. 6. The load and horizontal displacement were measured by the actuator. The specimens were whitewashed to observe the experimental phenomena during the tests.

4. Test results

The story drift ratio (θ_{el}), which can be used to express the capacity of the total rotation, is computed as the beam tip displacement over the distance from the actuator to the center of the column. The equation can be expressed as follows

$$\theta_{el} = \frac{\Delta}{L_{cb}} \times 100(\%) \tag{7}$$

where, Δ is the displacement of the loading point and L_{cb} is the distance from the column center to the loading point.

Total plastic rotation is obtained by subtracting the elastic portion of rotation from the total rotation. The elastic portion of rotation is calculated by dividing the applied load by the initial elastic stiffness of the beam, which can be expressed as follows

$$\theta_p = \frac{\Delta - P/K_i}{L_{cb}} \times 100(rad) \tag{8}$$

where, P is the applied load and K_i is the initial stiffness of the beam-to-column connections. The seismic performance of a beam-to-column connection is affected by the ultimate strength and the deformation capacity. The evaluation of strength can be expressed by the normalized moment, which can be illustrated by the ratio of M_f/M_p. M_p is the capacity of the beam plastic moment calculated from a section of the beam, M_f is the calculated moment, measured at the column face. The normalizing factor represents the maximum load magnitude at each level of story drift ratio.

4.1 Base specimen

During the cycles of 0.0075 rad drift, bolt slip occurred at the beam splice. The slip load was 116 kN. Very little flaking of the whitewash was observed on the beam flange near the groove weld. During the cycles of 0.01 rad drift, the whitewash began to flake on the beam flange near the groove weld. During cycles of 0.02 rad drift, flaking was observed on the beam web, starting at the extreme corners of the shear plate. The flaking subsequently spread along the length of the stub beam. Minor buckling of the beam web was also observed. This generally occurred near the beam splice but not near the beam-to-column joint. Minor cracks were also observed at the welding of the backing bar. During cycles of 0.04 rad drift, minor cracks also appeared at the welding of the shear plate around the weld access hole. Visible cracks appeared at the welding of the backing bar and obvious torsional buckling was also observed. In order to protect the actuator, this test was stopped. The maximum load was 251 kN. Experimental features are shown in Figs. 7(a)-(b), and hysteretic curves of the story drift ratio and total plastic rotation are provided in Figs. 8(a)-(b).

(a) Crack at the welding backing bar

(b) Lateral torsional buckling

Fig. 7 Experimental features of base specimen

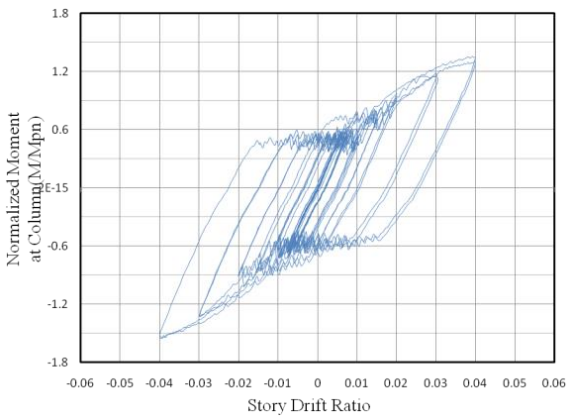

(a) Normalized moment versus story drift ratio

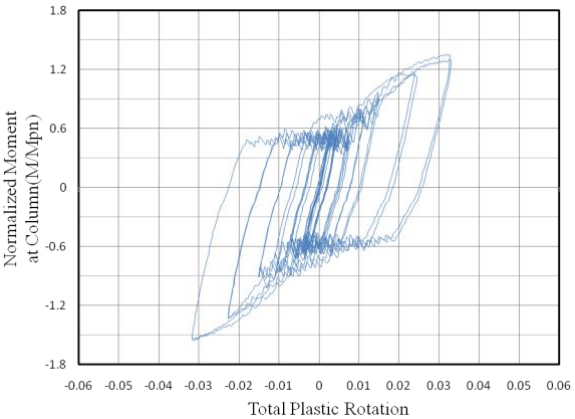

(b) Normalized moment versus total plastic rotation

Fig. 8 Hysteretic curves of base specimen

4.2 CTY600 specimen

The specimen remained in the elastic region until cycles of 0.0075 rad drift. At 0.01 rad drift, bolt slip occurred at the beam splice. The slip load was 140 kN. Little whitewash flaking was observed around the first row of bolts at the beam splice plate. During the cycles of 0.015 rad drift, in the region of the first row of bolts at the beam splice plate, whitewash flaking spread from the bolt to the middle of the beam splice plate with an angle of about 45 degrees. A small amount of whitewash flaking was then observed at the stub beam flange and the stiffener during cycles of 0.02 rad drift. Whitewash flaking of the stub beam flange spread from the root to the beam splice during 0.03 rad drift. Until the cycles of 0.04 rad drift, only whitewash flaking of the beam web was observed. At the final cycles of 0.05 rad drift, plate buckling was seen in the middle of the beam splice plate. The link beam also yielded. Gross section yielding of the stub beam web and local buckling of the beam web did not occur. The maximum load was 301 kN. Experimental features are shown in Figs. 9(a)-(c), and hysteretic curves of the story drift ratio and total plastic rotation are provided in Figs. 10(a)-(b).

(a) Cruciform yielding with an angle of 45 degrees

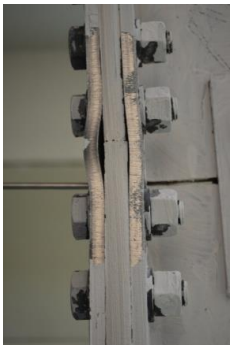

(b) Flange splice plates buckling

(c) Flanges and web of link beam yielding

Fig. 9 Experimental features of CTY600

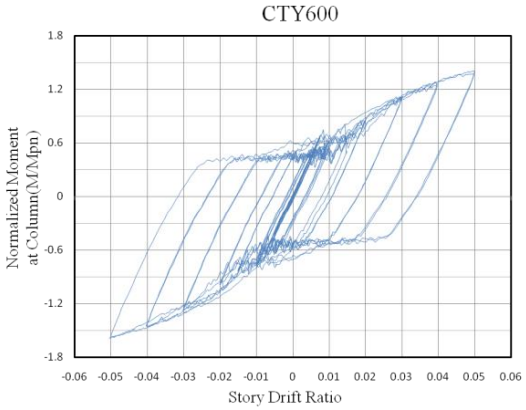

(a) Normalized moment versus story drift ratio

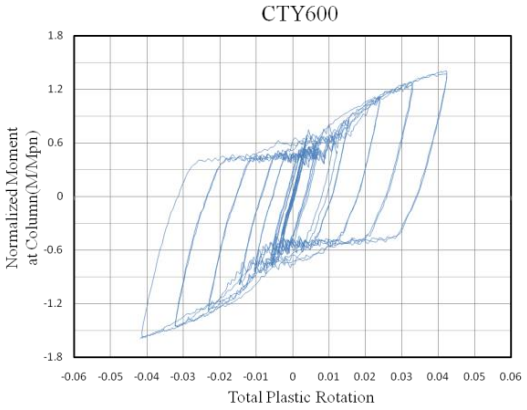

(b) Normalized moment versus total plastic rotation

Fig. 10 Hysteretic curves of CTY600 specimen

4.3 CTY900 specimen

Until the cycles of 0.0075 rad drift, the specimen remained in the elastic region. Starting at cycles of 0.01 rad drift, bolt slip occurred at the beam splice. The slip load was 138 kN. Little whitewash flaking was observed at the welding of stiffeners and at the root of the stub beam during the cycles of 0.01 rad drift. At 0.015 rad drift, very little whitewash flaking was observed in the region of the first row of bolts at the beam splice plate. During the cycles of 0.02 rad drift, the whitewash flaking was observed around the first row of bolts. The whitewash flaking of the flange splice plate spread with an angle of 45 degrees at 0.03 rad drift. During the cycles of 0.04 rad drift, whitewash flaking of the flange splice plate spread to the second row of bolt. During the final cycles of 0.05 rad drift, local buckling was observed in the middle of the beam splice plate. And around the beam splice plate, whitewash flaking was observed both at the stub beam and the link beam. Gross section yielding and local buckling of the splice connection were observed. Experimental features are shown in Fig. 11, and hysteretic curves of the story drift ratio and total plastic rotation are presented in Fig. 12.

(a) Cruciform yielding with an angle of 45 degree

(b) Flange splice plates buckling

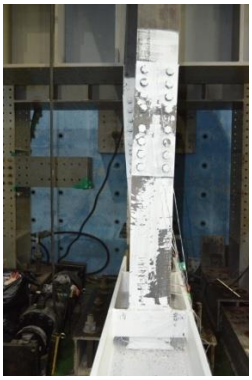

(c) Lateral torsional buckling

Fig. 11 Experimental features of CTY900 specimen

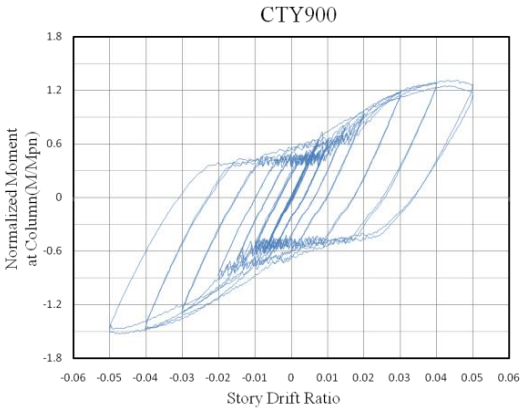

(a) Normalized moment versus story drift ratio

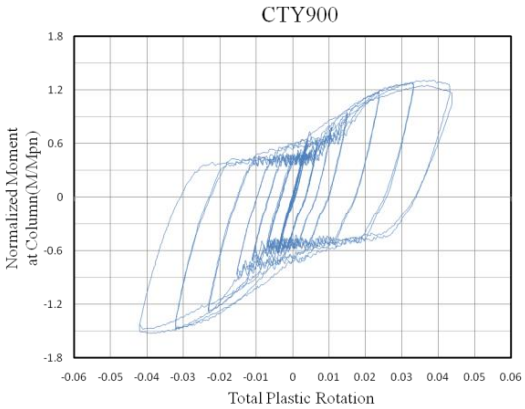

(b) Normalized moment versus total plastic rotation

Fig. 12 Hysteretic curves of CTY900 specimen

4.4 Summary of test results

The results showed that the CTY specimens developed ductile behavior without brittle fracture until a 0.05 rad story drift ratio and base specimen withstood a story drift ratio of 0.04 rad. The total plastic rotation exceeded 0.04 rad and over 0.03 rad drift respectively.

The initial stiffness obtained from CTY specimens was similar to that of the base specimen. Even though the thickness of the stiffener plates in the CTY specimens was smaller than that of base specimen, the hysteretic stiffness of the CTY specimens did not show visible loss. Regarding the column-tree connections, it could be concluded, that reducing the gross-sectional area of the splice plates does not have a large influence on the initial stiffness and stiffness retention.

The load of base specimen was 116 kN when the first slip occurred. The corresponding loads of the CTY600 and CTY900 specimens were 138 kN and 140 kN, respectively. In all tests bolt slip of the web splice occurred earlier than bolt slip of the flange splice. In order to make a thorough inquiry of the bolt slip in the beam splice, the load at the slip point was sampled and filtered based on a normal distribution. The load at the time of the first bolt slip and the average load of the filtered samples were summarized. The results showed that the average slip load and frequency were similar. The whitewash began to flake on the beam flange at 0.01 rad drift in base specimen test. Meanwhile, the same phenomenon was clearly observed after 0.02 rad drift in the CTY specimens. Instead of stub beam flange yielding, the flange splice plates yielded at an earlier time point and spread from the first row of bolts to the middle of beam splice plate with an angle of about 45 degrees. This delayed effect was also observed in the stub beam web.

The area of beam web yielding was mainly concentrated along the stub beam in the base specimen test. But that phenomenon were observed tests not only in the stub beam but also around the beam splice area even spread to the link beam in the CTY specimen. This showed that reducing the gross-sectional area of splice plates could delay the stub beam yielding and increase the plastic rotation capacity in the beam splice and a portion of the link beam.

Lateral torsional buckling took place in the base and CTY 900 specimens. This may be attributable to the location of the beam splice of the CTY600 specimen being smaller than that of base and CTY900 specimens. Moving closer to the location of the beam splice near the column, the extreme outermost bolts at the web splice plates require more slip resistance. The test results were summarized in Table 3.

Table 3 Summary of test results

Specimen	Base	CTY600	CTY900
Max. resistance strength(kN), P_u	293	301	288
Slip resistance strength(kN), P_s	115	108	104
Max. normalized moment, M_f/M_p	1.55	1.59	1.53
Max. story drift (rad), δ_t	0.04	0.05	0.05
Total plastic rotation (rad), θ_t	0.0319	0.0423	0.0437
Beam plastic rotation (rad), θ_b	0.0255	0.0350	0.0371
Stub beam plastic rotation (rad), θ_{sb}	0.0210	0.0216	0.0178
Link beam plastic rotation (rad), θ_{lb}	0.0045	0.0134	0.0193
Panel zone plastic rotation (rad), θ_{pz}	0.0064	0.0073	0.0066

5. Analysis of experimental results

5.1 Distribution of total plastic rotation

Most beam-to-column moment connections for SMF and IMF systems develop inelasticity in the panel zone and a plastic hinge in the beam. According to the requirements of Seismic Provisions for Structural Steel Buildings, beam-to-column connections used in special moment frames (SMFs) must be capable of sustaining a story drift ratio of at least 0.04 rad. In this regard, all specimens except for base specimen satisfy the requirements above.

The distribution rates of total plastic rotation between the panel zone, stub beam, and link beam was summarized in Fig. 13. As can be seen in weak-axis connections, the stub beam and link beam are in a great portion of maintaining the deformation capacity. Compared with the plastic rotation capacity at the link beam, the contribution rate in the CTY specimens was larger than that of base specimen. It showed that by reducing the cross-sectional area of the flange splice plates, the link beam can utilize more ductility capacity. With an increase of the splice location length, the available utilization would increase simultaneously. If the splice location has an appropriate length, this also can reduce the ductility requirements of beam-to-column joints.

5.2 Strain in the middle of flange splice plates

The relationship between stain parameters at the middle of the flange splice plates and the total load was shown in Fig. 14.

Bolt slip occurred during the two specimen tests. However, until cycles of 0.03 rad drift, the hysteretic curve remained stable and balanced. It indicated that minor bolt slip did not significantly affect the assumption of the moment distribution between the web plates and flange plates, and the neutral axis did not shift back. From cycles of 0.04 rad drift, both hysteretic curves shifted offset to one side. The periodic curves of the CTY900 specimen were completely yielding and with tension elongation over 20%. But the tension elongation of base specimen was only about 5%. By

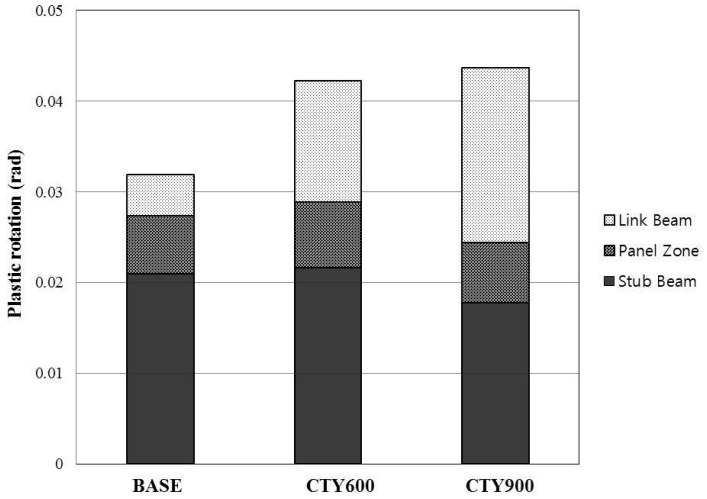

Fig. 13 Distribution of total plastic rotation

reducing the cross-sectional area of the flange splice plates, it is thus possible to fully exploit the ductility of the steel. This also explained why the CTY specimens could utilize more plastic rotation capacity of the link beam. In the case of inadequate flanges, moment exceeding the capacity of the flanges capacity must be carried by the web. Starting from cycles of 0.04 rad drift, the neutral axis was offset to one side, and consequently the assumption of elastic flexural theory no longer held. The extreme outermost bolts at the web splice plates should be more strictly check.

5.3 Energy dissipation capacity

The total accumulated energy dissipation of each specimen with increasing cycles is summarized in Fig. 15.

CTY specimens with different locations of beam splice exhibited almost the same energy dissipation capacity. CTY600 and CTY900 specimens both have larger energy dissipation capacity than the base specimen since these two specimens reached 0.05 rad total story drift. However, compared with the energy dissipation capacity at 0.04 rad story drift ratio as shown in Fig. 15(b), base specimen exhibited better performance than the CTY600 and CTY900 specimens. This

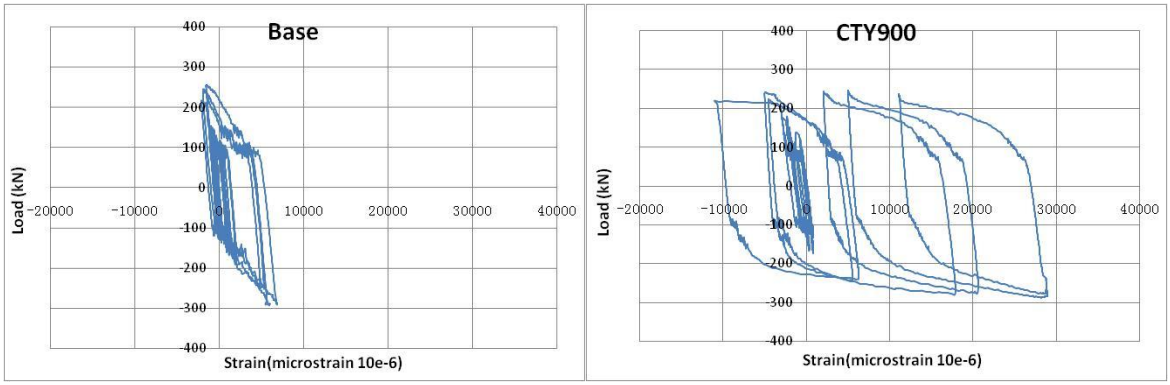

(a) Base specimen (b) CTY900

Fig. 14 Strain in the middle of flange splice plates

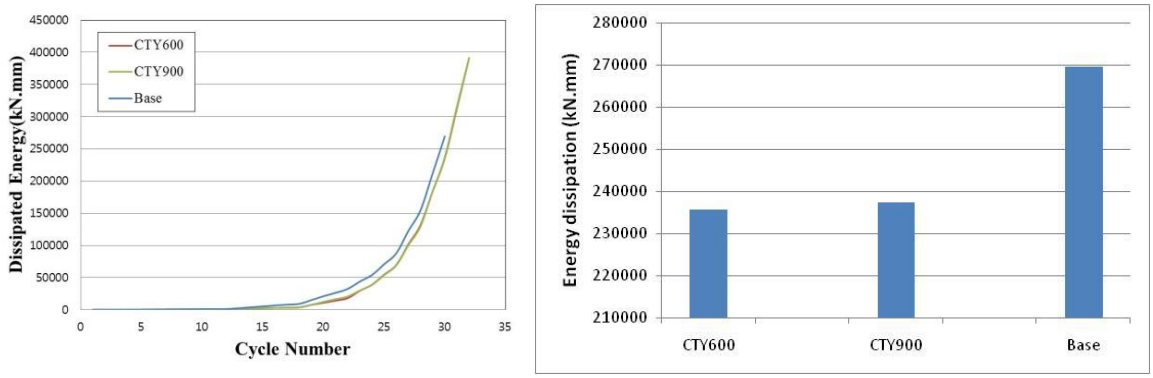

(a) Energy dissipation with increasing cycles

(b) Comparison of accumulated energy dissipation at 4% story drift ratio

Fig. 15 The accumulated energy dissipation of each specimen

might be attributable to the CTY specimens being able to utilize more deformation capacity of the beam splice including the material plastic deformation. As a result, the flanges and web of the stub beam could delay entry to the plastic deformation stage and also delay dissipation of cyclic energy. Reducing the cross-sectional area of the flange splice plates did not increase the energy dissipation capacity during the same story drift ratio.

6. Conclusions

Based on the experimental results and analysis, the following conclusions regarding weak-axis moment connections:

• The area of beam web yielding was mainly concentrated along the stub beam in the base specimen test. But in the CTY specimen tests distributed not only in the stub beam but also around the beam splice area and even spread to the link beam. Reducing the gross-sectional area of splice plates could delay the stub beam yielding and increase the plastic rotation capacity in the beam splice and a portion of the link beam. This also can reduce the ductility requirements of beam-to-column joints.

• The initial stiffness and maximum strength of the CTY specimens were similar to those of the base specimen. In column-tree connections, reducing the gross-sectional area of splice plates did not have a large influence on the initial stiffness, stiffness retention, or maximum strength.

• Reducing the cross-sectional area of the flange splice plates could make full use of the ductility of steel, and therefore make it possible to utilize more plastic rotation capacity of the link beam. Consequently, the flanges and web of the stub beam could delay entry into the plastic deformation stage and also delay dissipation of cyclic energy. Reducing the cross-sectional area of the flange splice plates did not increase the energy dissipation capacity during the same story drift ratio.

• In the case of inadequate flanges, moment exceeding the capacity of the flanges must be carried by the web. The neutral axis could be offset to one side, and hence elastic flexural theory did not meet the assumption. The extreme outermost bolts at the web splice plates must be strictly checked.

• Bolt slip occurred much earlier than expected in the web splice plates. This indicated that use of the elastic vector method is not suitable for the analysis of an eccentrically load bolted connection. To maintain stable and consistent web plates, it is recommended that adequate cross-sectional area be designed in order to carry total shear and excessive moment due to bolt slip.

• The CTY specimens successfully achieved a 5% story drift ratio without brittle fracture. The failure mode of these specimens was local buckling of the beam flanges. The specimens meet the qualification criteria required by the AISC Seismic Provisions.

Acknowledgments

This research was supported by the Basic Science Research Program through the National Research Foundation of Korea (NRF) funded by the Ministry of Education, Science and Technology (grant number: 2012R1A1A4A01004350).

References

AISC (2010), *Seismic provision for structural steel building*, American Institute of Steel Structure, Chicago, IL, USA.

Astaneh-Asl, A. (1997), "Seismic design of steel column-tree moment-resisting frames", *Structural Steel Educational Council*.

FEMA (2000), *Recommended Seismic Design Criteria for New Steel Moment-Frame Buildings: FEMA-350*, SAC Joint Venture, Richmond, Caliph, USA.

Han, S.W., Kwon, G.U. and Moon, K.H. (2007), "Cyclic behavior of post-Northridge WUF-B connections", *J. Constr. Steel Res.*, **63**(3), 365-374.

Hisashi, Okada, *et al*. (2001), *Recommendation for Design of Connections in Steel Structures*, Architectural Institute of Japan, Japan.

Kim, S.S., Lee, D.H. and *et al.* (2004), "Development of beam-to-column connection details with horizontal stiffness in weak axis of H-shape column", *J. Korean Soc. Steel Constr.*, **16**(5), 641-652.

KS B 0801 (2007), *Test Pieces for Tensile Test for Metallic Materials*, Korean Industrial Standards, Korea.

Lee, C.H. and Park, J.W. (1998), "Cyclic seismic testing of full-scale column-tree type steel moment connections", *J. Korean Soc. Steel Constr.*, **10**(4), 629-639.

Lee, K., Li, R., Chen, L., Oh, K. and Kim, K.S. (2014), "Cyclic testing of steel column-tree moment connections with various beam splice lengths", *Steel Compos. Struct.*, **16**(2), 221-231.

Mahin, S.T. (1998), "Lessons from damage to steel buildings during the Northridge earthquake", *Eng. Struct.*, **20**(4-6), 261-270.

McMullin, K.M. and Astaneh-Asl, A. (2003), "Steel semirigid column-tree moment resisting frame seismic behavior", *J. Struct. Eng.*, **129**(9), 1243-1249.

Miller, D.K. (1998), "Lessons learned from the Northridge earthquake", *Eng. Struct.*, **20**(4-6), 249-260.

Nader, M.N. and Astaneh-Asl, A. (1996), "Shaking table tests of rigid, semirigid, and flexible steel frames", *J. Struct. Eng.*, **122**(6), 589-596.

Tsai, K.C., Wu, S. and Popov, E.P. (1995), "Experimental performance of seismic steel beam-column moment joints", *J. Struct. Eng.*, **121**(6), 925-931.

CC